

CITRIC ACID CROSSLINKED NANOFIBRILLATED CELLULOSE FROM
BANANA (*MUSA ACUMINATA X BALBISIANA*) PSEUDOSTEM FOR
ADSORPTION OF Pb^{2+} AND Cu^{2+} IN AQUEOUS SOLUTIONS

JARED VINCENT T. LACARAN,^{*} RONALD JEFFERSON NARCEDA,^{*}
JOSANELLE ANGELA V. BILO^{**} and JULIUS L. LEAÑO JR.^{**}

^{*}*Chemistry Department, Adamson University, Ermita, Manila, 1000, Philippines*

^{**}*Research and Development Division, Philippine Textile Research Institute, Department of Science and
Technology, Bicutan, Taguig City, 1630, Philippines*

✉ *Corresponding author: J. A. V. Bilo, javbilo@gmail.com*

Received October 9, 2020

Nanofibrillated cellulose was isolated from banana pseudostem, a common agricultural waste, using acid hydrolysis and ultrasound irradiation and was thermochemically crosslinked with citric acid and used for the adsorption of Pb^{2+} and Cu^{2+} ions in an aqueous solution. The synthesized nanofibrillated cellulose was characterized using scanning electron microscopy (SEM), energy dispersive X-ray (EDX), Fourier-transform infrared spectroscopy (FTIR), and the analysis of the point of zero charges (PZC). The SEM data showed that nanofibrillated cellulose has a width of around 69 nm and the EDX spectra depicted the successful removal of inorganic constituents. The linkage of citric acid to cellulose was confirmed by FTIR and the analysis of the PZC revealed that citric acid modification imparted negatively charged carboxyl groups to the cellulose surface. The optimization of the solution pH and adsorbent dosage showed that 99% of Pb^{2+} and Cu^{2+} ions were removed under optimum conditions of pH 5 and 2.5 g/L of adsorbent, with high recyclability and following the Freundlich isotherm model. In addition, it was found that the adsorption process is exothermic, reversible, and driven by physisorption. The maximum adsorption capacity was found to be 205.42 mg/g for Pb^{2+} and 56.04 mg/g for Cu^{2+} , which makes CA-NFC comparable to existing citric acid modified agricultural wastes.

Keywords: banana pseudostem, citric acid crosslinked nanofibrillated cellulose, adsorption of Pb^{2+} and Cu^{2+} , Freundlich isotherm

INTRODUCTION

The release of heavy metal contaminants into the environment is a major global concern that has arisen because of irresponsible anthropogenic activities.¹ Heavy metals are highly toxic environmental contaminants that can disrupt the body's metabolic processes, even at extremely low concentrations.² Lead, a common heavy metal, can damage the skeletal and central nervous systems.³ Copper, another heavy metal, can impair the brain, kidneys and liver.⁴ Exposure to high amounts of heavy metals can eventually lead to death.⁵

With a view to removing heavy metal contaminants, various processes have been utilized, such as chemical precipitation, membrane processes, ion-exchange, filtration, and adsorption.¹ Among these processes, adsorption is

seen as the ideal method due to its effectiveness, low cost, and biocompatibility.⁶ However, because adsorption is a surface process, its efficiency may be limited by the adsorbent's surface area. This limitation can be overcome using nanotechnology by the production of nanoadsorbents with higher specific surfaces that can result in higher adsorption efficiency.⁷

Agricultural wastes are seen as ideal raw materials for the fabrication of nanoadsorbents because they have little economic value.⁸ Banana pseudostem is one of the most abundant agricultural wastes in our country. The Philippines, being the 5th largest banana producer worldwide, generates tons of pseudostem wastes, which are generally left to decompose by farmers.^{9,10} Banana pseudostem can be used as an

adsorbent for removing Pb^{2+} ions from aqueous solutions.¹¹ Nevertheless, agricultural wastes contain soluble organic compounds that are released during the adsorption process. As such, chemical modification is necessary to circumvent this risk.¹ The innate sorption ability of agricultural wastes results from the presence of numerous cellulosic groups found on the plant surface. Cellulose, a linear homopolysaccharide, is non-toxic, hydrophilic, and easily modified.¹² Furthermore, nanofibrillation and functionalization can greatly enhance the natural sorption ability of cellulose.¹³ Importantly, citric acid, a strong chelating agent, easily crosslinks with cellulose.¹⁴ Banana pseudostem has high cellulose content, making it a promising raw material for nanocellulose fabrication.¹⁵⁻¹⁷ In this work, nanofibrillated cellulose was extracted from the agricultural waste banana pseudostem, using acid hydrolysis and ultrasound irradiation, was thermochemically crosslinked with citric acid and further investigated for the adsorption of Pb^{2+} and Cu^{2+} ions in an aqueous solution.

EXPERIMENTAL

Materials and reagents

Banana (*Musa acuminata x balbisiana*) pseudostem samples were provided by the Philippine Textile Research Institute (PTRI), the Department of Science and Technology (DOST). Analytical grade NaOH, H_2O_2 , HCl, H_2SO_4 , HNO_3 , NaOCl, Na_2SO_3 , CH_3COONa , CH_3COOH , Na_2EDTA , citric acid, Pb (II) nitrate and Cu (II) nitrate were purchased from Sigma, and used in this study without purification.

Synthesis of nanofibrillated cellulose modified with citric acid (CA-NFC)

Isolation of α -cellulose

The outer part of the banana pseudostem was stripped by hand and the fiber component was extracted using a decorticating machine. The extracted fiber was degummed by boiling in 12% NaOH for 2 hours and then in 8 g/L peroxide solution. The samples were neutralized using 1% HAc and treated again in 6% NaOH and peroxide. The samples were neutralized and washed 3 times with hot water. The particle size of the fiber was reduced by milling in a Thomas Scientific Wiley mill with a 20 mesh sieve. The fiber was delignified by boiling in 2% Na_2SO_3 for 10 minutes and bleaching in a 10% sodium hypochlorite and 10% sulfuric acid solution for 10 minutes before washing with hot water. The delignification process was repeated twice until the fiber became completely white. The delignified fiber was soaked in 17.5% NaOH for 35 minutes and in 8% NaOH for 30 minutes. The fiber was then neutralized with 10% HAc and

washed with distilled water before drying. The process was repeated several times to purify the isolated α -cellulose.

Nanofibrillation of α -cellulose

The dried α -cellulose was hydrolyzed at 45 °C in HCl, with concentrations of 12 M for 1 hour, 7.5 M for 2 hours, and 6 M for 1 hour. The solution was quenched with NaOH and washed with distilled water until the pH became neutral. The α -cellulose was sonicated (Chromtech UC-20500BDT Ultrasonic Cleaner) at 60 kHz for 1 hour, followed by centrifugation (Hermle Z206A centrifuge) at 6000 rpm for 15 minutes and dried for 48 hours at 80 °C.

Thermochemical crosslinking with citric acid

Nanofibrillated cellulose (NFC) was mixed with 1.2 M citric acid and stirred at 500 rpm for 3 hours. The solution was filtered to remove excess citric acid and dried for 48 hours at 60 °C. The fiber was then heated for 3 hours at 150 °C and 400 mBar, and washed with hot distilled water until the pH of the washings became neutral. The washings were mixed with an equal amount of 20 mM Pb (II) nitrate buffered to pH 4.8 in a buffer solution of 0.03 M acetic acid and 0.07 M sodium acetate until no turbidity or cloudiness from the formation of lead (II) citrate due to unreacted citric acid was observed. The modified fiber was then dried for 72 hours at 60 °C. The product is from here on referred to as CA-NFC or citric acid crosslinked nanofibrillated cellulose.

Characterization

Energy dispersive X-ray (EDX)

The elemental composition of the fibers was investigated using a Phenom XL Energy Dispersive Spectroscopy Detector.

Fourier transform infrared spectroscopy (FTIR)

The functional groups present in the fibers were analyzed with a Bruker Tensor 27 Fourier-Transform Infrared Spectrometer with a crystal Attenuated Total Reflectance attachment in the range from 400 cm^{-1} to 4000 cm^{-1} .

Scanning electron microscopy (SEM)

To analyze the surface morphology, degummed banana fiber and cellulose were sieved and analyzed using a Phenom XL Scanning Electron Microscope. NFC was coated in gold nanoparticles, using a JEOL JFC-1200 Fine Coater and analyzed using JEOL 5310 SEM.

Point of zero charge (PZC)

The point of zero charge (PZC) was analyzed to determine the surface charge of the adsorbent.^{11,18,19} Deionized water was boiled for 20 minutes to remove dissolved CO_2 and 15 mL was transferred to vials containing 0.2 grams of NFC and CA-NFC. The vials

were quickly capped to prevent the dissolution of CO₂ and agitated for 3 days. Using a HORIBA LAQUA PC1100 Water Analyzer, the pH of the solutions was measured and recorded as the PZC.

Adsorption studies

Batch sorption experiments (triplicates) were conducted at a room temperature of 25 °C and the contact time was set to 3 hours to ensure equilibrium was reached. Deionized water was used in all adsorption experiments and dilute nitric acid and sodium hydroxide solutions were used for pH

adjustment. The solutions were vacuum-filtered using a 40-μM Gooch glass crucible filter. The concentrations of metal ions were measured using a Shimadzu AA-7000F Flame Atomic Absorption Spectrophotometer (F-AAS).

The removal efficiencies (%) and adsorption capacities (mg/g) were calculated using the equations in Table 1, where: C_o and C_e are the initial and equilibrium metal ion concentrations, respectively (mg/L), V is the volume (L), and W is the adsorbent weight (g).

Table 1
Adsorption equations

Removal efficiency (%)	$\frac{C_o - C_e}{C_o} \times 100$
Adsorption capacity (mg/g)	$\frac{(C_o - C_e)V}{W}$

Effect of pH

To investigate the influence of pH on metal ion adsorption, experiments at an initial pH of 3, 4, and 5 were conducted. In a conical flask, 0.25 g of NFC and CA-NFC were mixed with 100 mL of separate solutions containing 20 mg/L of Pb²⁺ and Cu²⁺. The solutions were magnetically stirred at 200 rpm and 25 °C before filtration and F-AAS analysis.

Effect of adsorbent concentration

The influence of adsorbent concentration was investigated using concentrations of 0.5, 1.5, and 2.5 g/L of adsorbents. The appropriate concentrations of NFC and CA-NFC were mixed with 100 mL of separate solutions containing 20 mg/L of Pb²⁺ and Cu²⁺ at pH 5. The solutions were magnetically stirred at 200 rpm and 25 °C before filtration and F-AAS analysis.

Adsorption isotherm

The isotherm model gives an insight into the mechanism of the adsorption process. It was determined by plotting the adsorption capacity of CA-NFC against solutions of increasing metal ion concentrations. For this study, the Freundlich, Langmuir, and Temkin isotherm models were evaluated using linear curve-fitting. The R² values of the models were compared and a Chi-square test was conducted to determine which model fits best.

Solutions with concentrations of approximately 20, 50, 100, 250, and 600 mg/L were prepared to properly model the adsorption process. 0.125 g CA-NFC was mixed in a polypropylene centrifuge tubes with 50 mL metal ion solution at pH 5 and shaken in a Daihan

Scientific shaking water bath at 150 rpm and a temperature of 25 °C ± 0.1 °C for 3 hours. The solutions were filtered and analyzed using F-AAS.

The isotherm was determined using the linearized form of the Freundlich, Langmuir, and Temkin models and evaluated by conducting Chi-square (χ²) statistical test. The equations used are shown in Table 2, where the Freundlich constant K_F represents the relative adsorption capacity of the adsorbent, $1/n$ is a measure of the adsorption intensity,⁵ K_L represents the Langmuir energy constant, q_m is an estimate of the adsorbent's maximum adsorption capacity,²⁰ K_T is the Temkin constant, b_T is the constant related to the heat of adsorption through $b_T = -\Delta H$, T is the absolute temperature (K), R is the universal gas constant (8.314 J/mol),²¹ C_e is the equilibrium metal ion concentration, q_e is the experimental adsorption capacity, and $q_{e,m}$ is the adsorption capacity calculated by the model.⁵

Regeneration and desorption

To investigate the regeneration of the adsorbent, 0.25 g of CA-NFC was mixed in a 100-mL conical flask with 100 mL of 20 mg/L metal ion solution. It was magnetically stirred for 3 hours before vacuum filtration. The adsorbent was recovered and underwent desorption in 100 mL of 0.05 M of NA₂EDTA for 90 minutes. The mixture was filtered and the adsorbent was washed with 100 mL of distilled water. The adsorbent was recycled twice and the removal efficiency (%) in each cycle was calculated.

Table 2
Isotherm equations

Freundlich model	$\log q_e = \log K_f + \frac{1}{n} \log C_e$
Langmuir model	$\frac{C_e}{q_e} = \frac{C_e}{q_m} + \frac{1}{q_m K_L}$
Temkin model	$q_e = \frac{RT}{b_T} \ln K_T + \frac{RT}{b_T} \ln C_e$
Chi-square test	$\chi^2 = \sum \frac{(q_e - q_{e,m})^2}{q_{e,m}}$



Figure 1: Stages of the physicochemical treatments

RESULTS AND DISCUSSION

Isolation, nanofibrillation and modification of cellulose

Isolation of cellulose

A combination of physical and chemical treatments was used to fully remove organic and inorganic constituents from the fiber and isolate cellulose.

Decortication is a common technique used in the processing of natural fibers, such as banana, abaca, pineapple and water hyacinth. It was used to remove the non-fibrous components of the pseudostem, such as the cortex, gums, waxes and natural dyes.²²

The alkali-based degumming process removes and solubilizes natural gums, waxes, resins, and other impurities from the fiber.²³ Peroxide bleaching whitens the fiber by oxidizing and decolorizing natural dyes and other impurities that

were not removed during the initial alkali treatment. During scouring, non-cellulosic constituents are removed by the breakdown of residual phenolic compounds.^{15,24} After degumming and bleaching, the fiber changed in color from brown to a yellowish-white, indicating removal of impurities.²⁵

Delignification was accomplished by combining sulfite pulping with hypochlorite bleaching to solubilize lignin by cleaving lignin bonds. The fiber turned white as a result of the decolorization of lignin and oxidation of the lignin chromophores.²⁶

The treatment of delignified fibers with 17.5% NaOH separates the high-molecular-weight cellulose, known as α -cellulose, from hemicelluloses and other short-chain carbohydrates entangled in the fiber matrix.¹² The resulting cellulose isolate was pure white and powdery in appearance.

Nanofibrillation of cellulose

Under controlled conditions, the treatment with a strong acid, such as HCl, at high temperatures, solubilizes the disordered and amorphous regions in the polymer structure of cellulose and leaves behind the crystalline regions, which have a higher resistance to acid.¹² Acid hydrolysis yielded shorter fibers as a result of acid protons attacking cellulosic oxygens, resulting in slow cleavage of the glycosidic bonds.²⁷

Ultrasound irradiation is a mechanical process that uses oscillating sound waves to produce acoustic cavitation or the creation and violent collapse of vacuum bubbles in a liquid. Acoustic cavitation generates shockwaves and microjets that isolate cellulose nanofibrils upon impact by the scission and disintegration of the weak van der Waals forces holding the fiber bundles together. This results in the individualization of the nanofibrils, molecular weight reduction, and a higher surface area, which makes it ideal for nano-adsorption.^{12,28} After ultrasound irradiation, cellulose lost its cotton-like texture and became

more crystalline and granular, indicating a reduction of the amorphous regions.²⁷

Thermochemical crosslinking with citric acid

The reaction of citric acid with cellulose is described as a thermochemical reaction because of the necessity of using heat to form an ester bond between citric acid and the cellulose hydroxyls. The application of heat dehydrates the citric acid and condenses it into an anhydride derivative. The highly-reactive citric acid anhydride will then form an ester linkage with the cellulose hydroxyl groups and, upon further heating, condenses again to crosslink two cellulose molecules.^{29,30} Crosslinking also attaches negatively charged carboxyl groups into the cellulose backbone and increases the material's capacity to bind metal cations.^{19,31,32} After crosslinking, the color of the nanofiber became the characteristic yellow that is associated with natural fibers linked with citric acid.³³ Its effect on the adsorption efficiency of cellulose was investigated in the succeeding adsorption experiments.

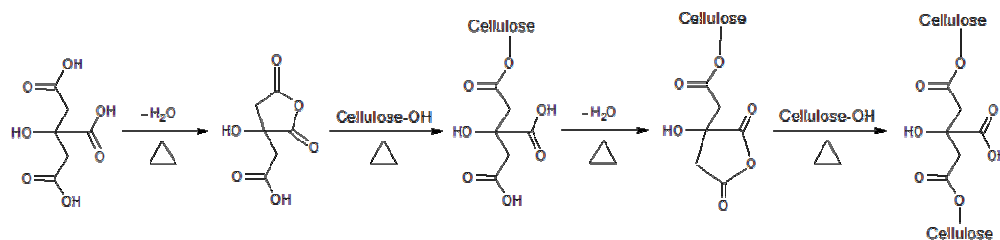


Figure 2: Reaction mechanism of crosslinking of citric acid with cellulose

Characterization results

Energy dispersive X-ray (EDX)

Energy dispersive X-ray analysis was used to determine the elemental composition of fibers. It was found that degumming successfully removed inorganic constituents from the fiber, such as potassium and calcium. The isolated cellulose fiber was found to contain only carbon and oxygen, which corresponds to the composition of cellulose.³⁴

Fourier-transform infrared spectroscopy (FTIR)

Figure 4 shows the change in functional groups with each pretreatment process. The strong

peaks from 1200 cm^{-1} to 1500 cm^{-1} are due to the C=C stretching of aromatic rings. The strong peak at 1000 cm^{-1} is due to C-O-C vibrations. The peak at 2800 cm^{-1} is due to the vibration of sp^3 carbons. The broad peak from $3000\text{--}3600\text{ cm}^{-1}$ is due to the stretching of the hydroxyl groups. The OH stretch shortened with each treatment stage as a result of the removal of the hydroxyl-rich lignin and hemicelluloses. The peak at 1700 cm^{-1} is attributed to the C=O stretching of the acetyl and ester groups of hemicelluloses and lignin, which visibly shortened with each pretreatment.^{11,23,34,35} Citric acid crosslinking was confirmed by the strong C=O stretch on CA-NFC.^{29,30,33}

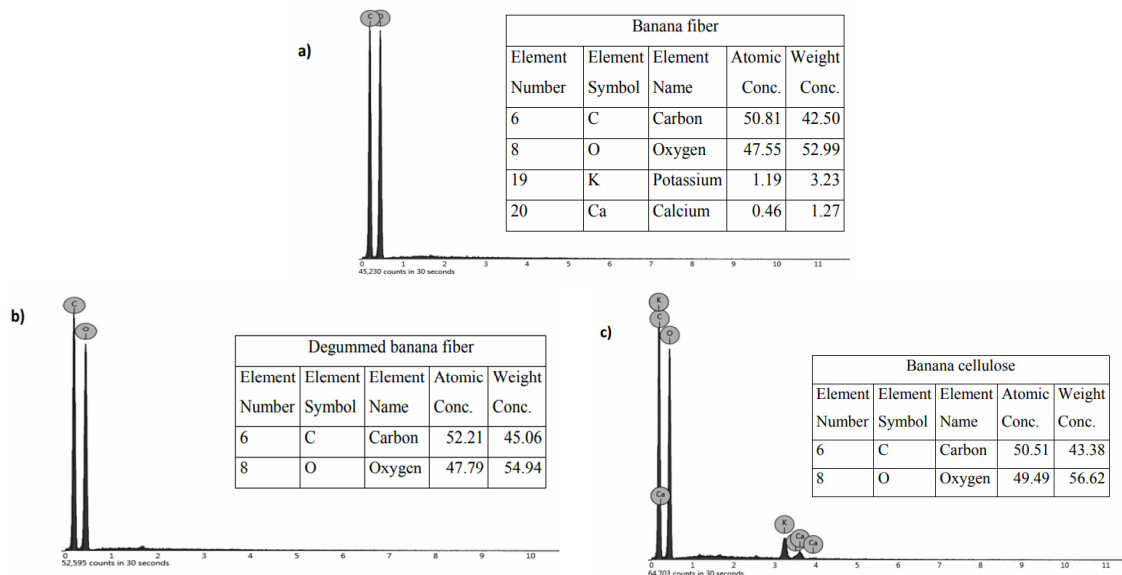


Figure 3: EDX profile and elemental composition of a) banana fiber, b) degummed fiber and c) banana cellulose

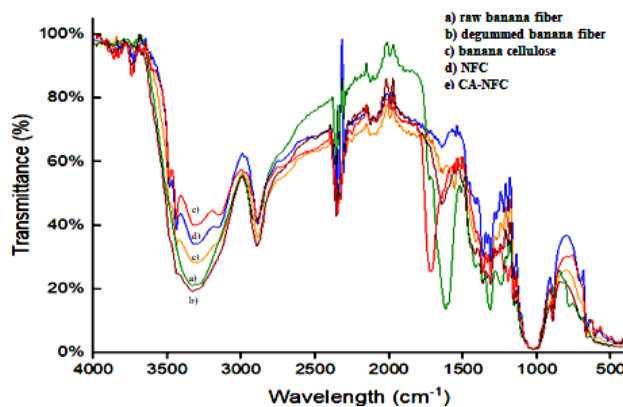


Figure 4: FTIR spectra of the a) raw banana fiber, b) degummed banana fiber, c) banana cellulose, d) nanofibrillated cellulose, and e) citric-acid modified nanofibrillated cellulose

Scanning electron microscopy (SEM)

Scanning electron microscopy showed that with each pretreatment step, a decrease in fiber width was observed due to the disentanglement of fiber bundles and stripping away of non-cellulosic impurities. The initial width of the untreated banana pseudostem fiber was around 148 μm . After degumming, the fiber width visibly decreased to around 12.9-19.1 μm . The cellulose that was isolated after delignification and alkali treatment had fibrils with widths of around 8.05-15.9 μm . Nanofibrillation using acid hydrolysis and ultrasound irradiation drastically reduced the fiber width to around 69 nm. Fibers with widths below 100 nm are known as nanofibrillated cellulose.³⁶

Point of zero charge (PZC)

The PZC was found to be 5.42 for NFC and 3.27 for CA-NFC. The PZC is the pH at which the surface charge of the material is neutral or equal to zero. When $\text{pH} = \text{PZC}$, there is no electrostatic interaction between the adsorbent surface and cations in the solution. At a pH higher than the PZC, the adsorbent is negatively charged and has a high affinity for metal cations. As such, chemically modified adsorbents with lower PZC are more ideal because they can adsorb metal ions at a greater pH range.^{11,18,19} The lower PZC of CA-NFC means that its surface is more negatively charged than NFC and contains a higher number of acidic sites due to the presence of weakly acidic oxygens.^{1,18,37}

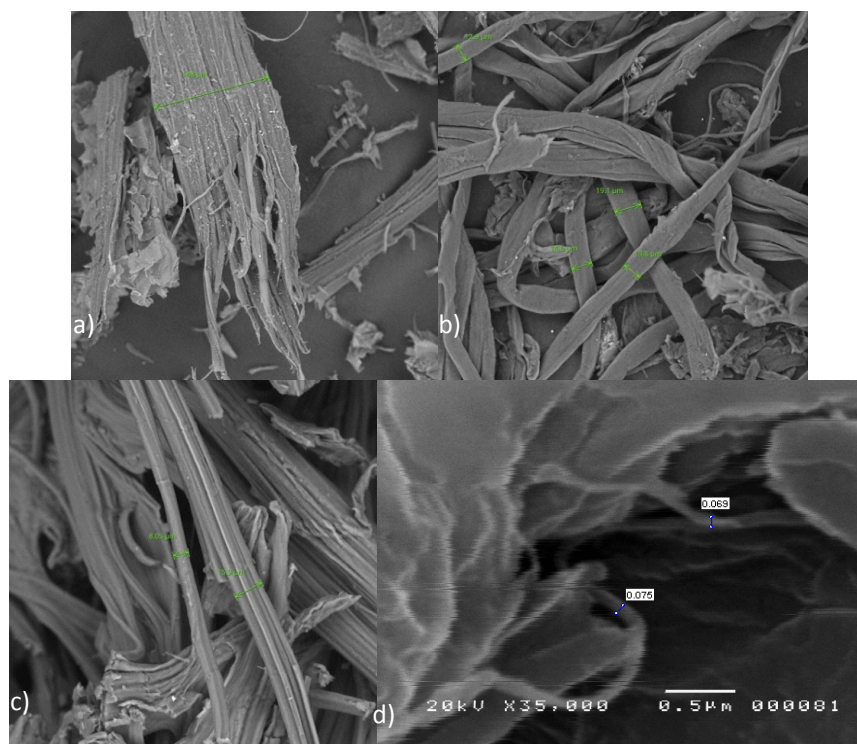


Figure 5: SEM images of a) banana fiber, b) degummed banana fiber, c) banana cellulose, and d) nanofibrillated cellulose

Adsorption experiments

Effect of solution pH

Solution pH can directly affect the surface charge of the adsorbent, the ionization of the functional groups, and the phase of the adsorbate. From Figure 6, it can be seen that the adsorption efficiency increased at higher pH levels. The low efficiency at low pH results from mobile H^+ ions competing with Pb^{2+} and Cu^{2+} for binding sites.³⁸ At higher pH, the unionized COOH group in CA-NFC deprotonates into the negatively charged COO^- , which has a higher affinity for metal cations.³⁹ Furthermore, surface charge also plays a key role in adsorption efficiency. At a pH lower than the PZC, the adsorbent has a low surface negative charge, which constrains metal ion adsorption because of electrostatic repulsions. It has also been observed that the initial solution pH decreases after contact time. This signifies that the ion-exchange mechanism also occurs on the adsorbent surface due to the release of H^+ ions.^{18,37,40}

Effect of adsorbent concentration

From Figure 7, it can be seen that increasing the adsorbent concentration results in an increase

in removal efficiency. For both adsorbents, maximum efficiency was achieved at an adsorbent concentration of 2.5 g/L with CA-NFC exhibiting 99% removal for Pb^{2+} and Cu^{2+} . This is attributed to the greater number of active sites available for metal sorption due to the increase in adsorptive surface area.^{5,11,41}

Adsorption isotherm

Equilibrium isotherm is an important parameter used in the determination of the possible mechanism of adsorption. It is also used to further understand the behavior of the adsorbent and its maximum adsorption capacity.⁴²

Freundlich isotherm model

The Freundlich isotherm model assumes that the adsorption process follows a multilayer mechanism on a heterogeneous adsorbent surface. A $1/n$ value between 0 and 1 indicates favorable adsorption capacity.⁵ A high K_F value indicates high adsorption capacity.³⁹ The $1/n$ and K_F values obtained show that the adsorption is favorable for both metals, but it is more favorable for Pb^{2+} than for Cu^{2+} . The high R^2 value obtained indicates high linearity.

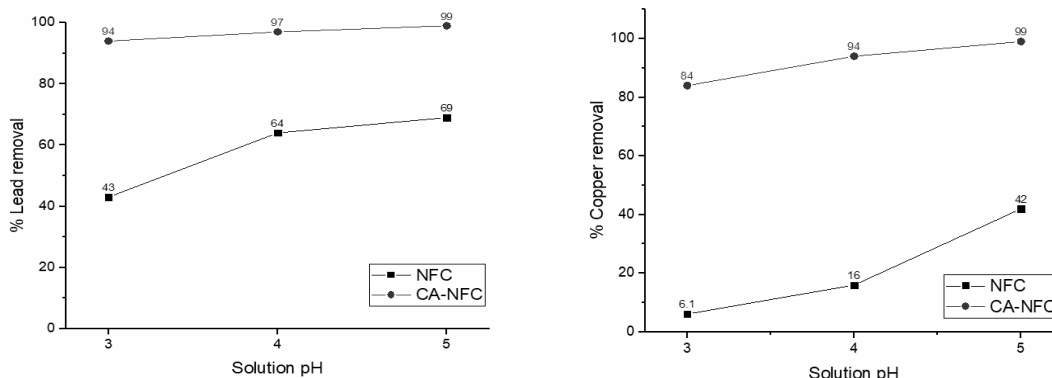


Figure 6: Effect of initial pH on Pb^{2+} and Cu^{2+} adsorption

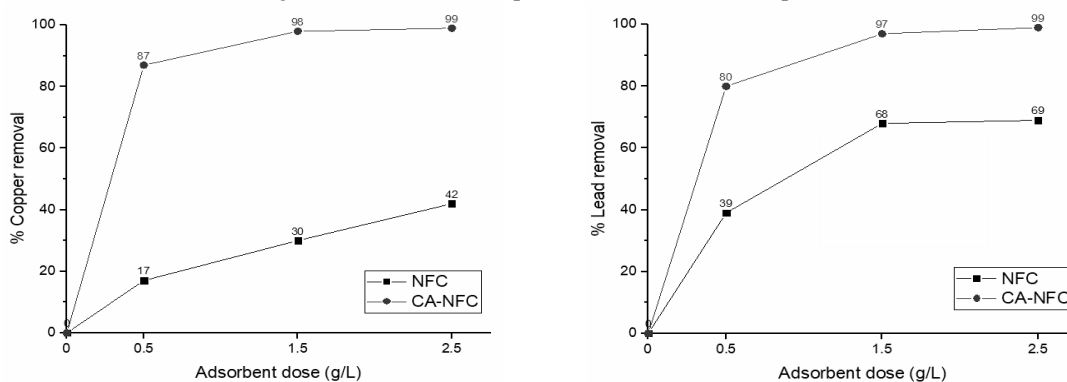


Figure 7: Effect of adsorbent concentration on Pb^{2+} and Cu^{2+} adsorption

Langmuir isotherm model

The Langmuir isotherm model is based on the assumption that the adsorption process follows a monolayer mechanism on a homogenous surface.^{37,40} As with the Freundlich model, it was found that the adsorption process favors Pb^{2+} more than Cu^{2+} , as evidenced by the higher q_m value for Pb^{2+} .

Temkin isotherm model

The Temkin isotherm model studies the heat of adsorption based on surface interaction between the adsorbent and the adsorbate. Similar to the Langmuir model, the adsorption process for the Temkin model occurs in a monolayer mechanism.²¹ Because b_T is positive, the adsorption process was determined to be exothermic. Additionally, b_T values less than 8 kJ/mol indicate weak adsorbate-adsorbent interactions. Hence, it is concluded that the adsorption process is reversible and driven by physisorption.⁴³

Chi-square (χ^2) test

The Chi-square statistical method was used to evaluate the fit of the isotherm by comparing the equilibrium capacities of the experiment and the model. If the experimental q_e is close to the value calculated by the model, the resulting χ^2 value will be small. Unlike the analysis of linearity using R^2 , the Chi-square test compares data points based on the same abscissa and ordinate. Through this, the best-fitting model can be determined.⁴⁴ The obtained χ^2 values are shown in Table 6. The order of the χ^2 values was Langmuir > Temkin > Freundlich. This indicates that the Freundlich isotherm is the best-fitting model as it has the lowest χ^2 value.⁵ Thus, the Freundlich isotherm is determined to be the best-fitting model and that the adsorption process follows a heterogenous, multilayer mechanism.

Regeneration and desorption

The adsorbent's regeneration was investigated because high regeneration is a characteristic of an

excellent adsorbent.⁴⁵ EDTA was used for desorption because its formation constants with Pb^{2+} and Cu^{2+} ($\log K_{\text{Pb-EDTA}} = 18.04$; $\log K_{\text{Cu-EDTA}} = 18.8$) are higher than those of citric acid ($K_{\text{Pb-CA}} = 4.1$; $K_{\text{Cu-CA}} = 6.1$).⁴⁶ This means that EDTA can easily regenerate CA-NFC by removing metal ions bound on the adsorbent surface.

From Figure 11, it can be seen that the adsorbed metal ions were desorbed by EDTA and

CA-NFC has high regeneration due to the removal efficiency still being above 90%, even after the third cycle. The easy removability of the adsorbed metals also confirms the assessment that the process is reversible and driven by physisorption.³² The high regeneration shows CA-NFC to be superior to activated carbon, which loses around 50% of its activity after the first regeneration.⁷

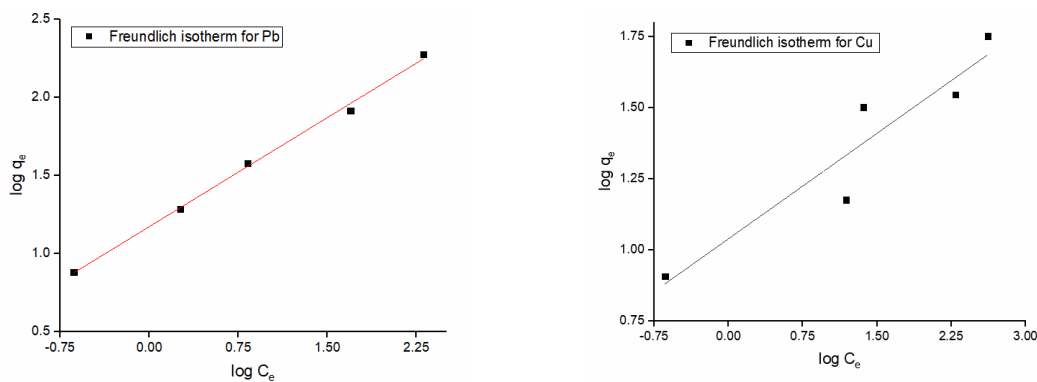


Figure 8: Freundlich plots for Pb^{2+} and Cu^{2+}

Table 3
Freundlich values

Freundlich isotherm model			
Metal	K_F	$1/n$	R^2
Pb^{2+}	14.85	0.47	0.997
Cu^{2+}	10.81	0.25	0.891

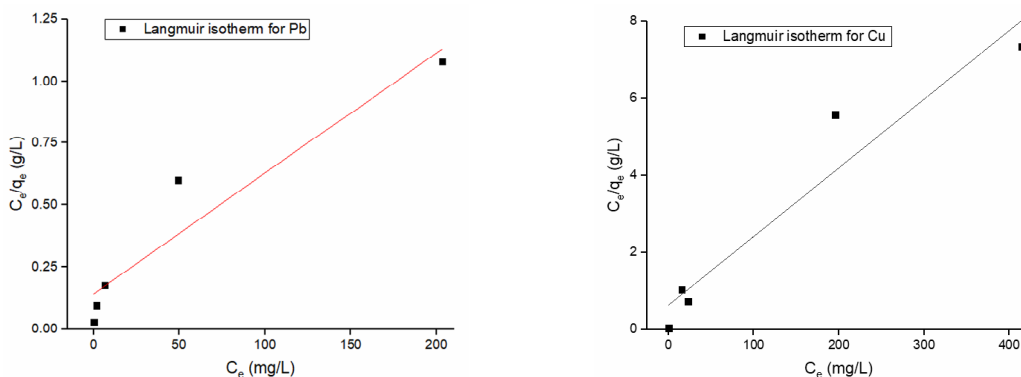


Figure 9: Langmuir plots for Pb^{2+} and Cu^{2+}

Table 4
Langmuir values

Langmuir isotherm model			
Metal	q_m (mg/g)	K_L (L/mg)	R^2
Pb^{2+}	205.42	0.034	0.915
Cu^{2+}	56.04	0.028	0.930

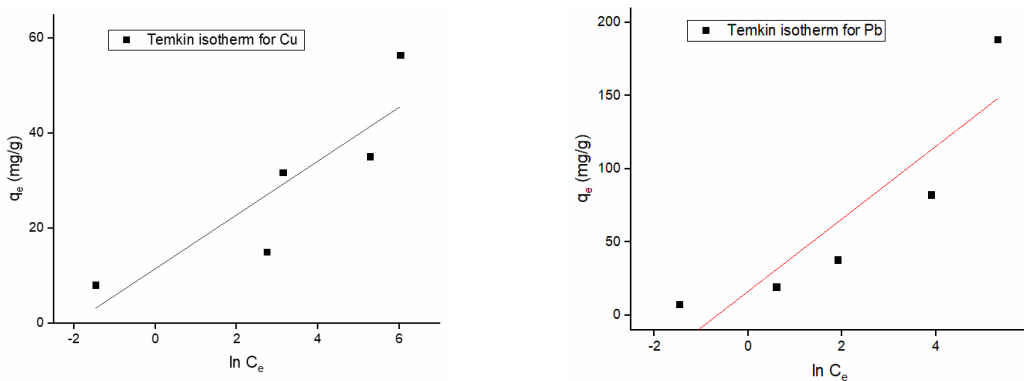


Figure 10: Temkin plots for Pb²⁺ and Cu²⁺

Table 5
Temkin values

Temkin isotherm model			
Metal	b_T (J/mol)	K_T (L/mg)	R^2
Pb ²⁺	100.162	1.93	0.809
Cu ²⁺	432.97	7.08	0.772

Table 6
Chi-square values

χ^2 values			
Metal	Freundlich	Langmuir	Temkin
Pb ²⁺	22.36	93.05	48.75
Cu ²⁺	6.64	159.13	19.53

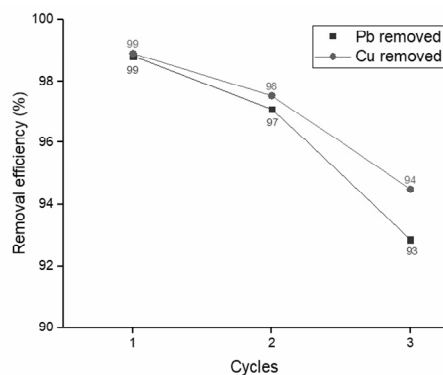


Figure 11: Adsorbent regeneration

Adsorbent affinity

The adsorption of metal ions in solution is governed by intrinsic properties such as ionic potential and the hydrated ionic radii. An ion’s radius is inversely proportional to its ionic potential. Consequently, ions with small radii attract more water molecules. This results in an inverse relationship between the ionic radius and the hydrated ionic radius, as the ions grow substantially larger due to attraction to the surrounding water molecules.^{44,47} The ionic radii

and hydrated ionic radii of Pb²⁺ and Cu²⁺ are shown in Table 7.

It was initially observed that the adsorption process exhibited a greater affinity for Pb²⁺ than Cu²⁺. This is explained by the respective intrinsic properties of the metals. The smaller hydrated ionic radius for Pb²⁺ means that it is absorbed more easily compared to Cu²⁺ due to the relatively small distance between the metal ion and the adsorbent surface.^{44,47}

Comparison with different adsorbents

The Langmuir q_m values of various adsorbents are summarized in Table 8. It can be seen that CA-NFC is comparable to different agricultural

and cellulosic adsorbents reported in the literature. For adsorbents that utilized both metals, the q_m values for Pb^{2+} are always consistently higher than the values for Cu^{2+} .

Table 7
Ionic radius of metal ions

Ion	Ionic radius (Å)	Hydrated ionic radius (Å)
Pb^{2+}	1.19	4.01
Cu^{2+}	0.73	4.19

Table 8
Maximum uptake (q_m) of various adsorbents

Adsorbent	Modification	Pb^{2+} uptake (mg/g)	Cu^{2+} uptake (mg/g)
Nanofibrillated cellulose from banana pseudostem (this study)	Citric acid	205.42	56.04
Corncoobs ¹⁹	Citric acid	118.104	42.58
Pine wood ⁴⁸	Citric acid	82.64	23.70
Sawdust ⁴⁹	Citric acid	38.332	11.18
Banana peels ⁴³	–	2.18	–
Banana pseudostem ¹¹	–	34.21	–
Newspaper ⁴⁰	Citric acid	34.6	–
Cellulose ³²	Citric acid	41.67	–
Soybean hulls ³¹	Citric acid	–	108
Orange peels ¹⁸	Citric acid	–	77.53
Soybean straw ³⁹	Citric acid	–	48.81

CONCLUSION

Nanofibrillated cellulose was crosslinked with citric acid through a facile thermochemical method to produce an adsorbent capable of removing 99% of Pb^{2+} and Cu^{2+} at optimum conditions of pH 5 and 2.5 g/L concentration. SEM analysis revealed that nanofibrillation was successful, as the cellulose nanofibrils exhibited a width of around 69 nm. The removal of inorganic constituents during the pretreatment process was confirmed by EDX analysis. FTIR spectroscopy revealed the removal of functional groups associated with organic impurities and the linkage of citric acid with cellulose by the intense carbonyl peak at 1700 cm^{-1} . Isotherm studies showed that the adsorption process followed the Freundlich model, indicating multilayer adsorption. The adsorption process was also found to be exothermic, reversible, and driven by physisorption. The maximum adsorption capacity was found to be 205.42 mg/g for Pb^{2+} and 56.04 mg/g for Cu^{2+} , making CA-NFC comparable to existing agricultural wastes modified with citric acid for adsorption applications. The analysis of adsorbent regeneration showed that CA-NFC exhibited a minimal change in efficiency, even

after 3 cycles. The adsorption process was found to greatly favor the removal of lead over copper as a result of their hydrated ionic radius. Overall, the total results prove that CA-NFC is an ideal nanoadsorbent.

REFERENCES

- W. S. Ngah and M. A. K. M. Hanafiah, *Bioresour. Technol.*, **99**, 3935 (2008), <https://doi.org/10.1016/j.biortech.2007.06.011>
- J. O. Duruibe, M. O. C. Ogwuegbu and J. N. Egwurugwu, *Int. J. Phys. Sci.*, **2**, 112 (2007), <https://doi.org/10.5897/IJPS.9000289>
- L. J. Thompson, in “Veterinary Toxicology”, edited by R. C. Gupta, Academic Press, 2018, pp. 439-444, <https://doi.org/10.1016/C2016-0-01687-X>
- G. F. Riedel, in “Encyclopedia of Ecology”, edited by S. E. Jørgensen and B. D. Faith, Elsevier Science, 2008, pp. 778-783, <https://doi.org/10.1016/B978-008045405-4.00380-3>
- R. Karthik and S. Meenakshi, *Chem. Eng. J.*, **263**, 168 (2015), <https://doi.org/10.1016/j.cej.2014.11.015>
- W. Shen, S. Chen, S. Shi, X. Li, X. Zhang *et al.*, *Carbohydr. Polym.*, **75**, 110 (2009), <https://doi.org/10.1016/j.carbpol.2008.07.006>
- K. R. Kunduru, M. Nazarkovsky, S. Farah, R. P. Pawar, A. Basu *et al.*, in “Water Purification”, edited by A. M. Grumezescu, Academic Press, 2017, pp. 33-

- 74, <https://doi.org/10.1016/B978-0-12-804300-4.00002-2>
- ⁸ V. G. Guptha, P. J. M. Carrott, R. Singh, M. Chaudhary and S. Kushwaha, *Bioresour. Technol.*, **216**, 1066 (2016), <https://doi.org/10.1016/j.biortech.2016.05.106>
- ⁹ Philippine Statistics Authority, in “Major Crops Statistics of the Philippines”, Philippine Statistics Authority, 2015, pp. 119-150
- ¹⁰ A. B. Guerrero, P. L. Aguado, J. Sánchez and M. D. Kurt, *Waste Biomass Valoriz.*, **7**, 405 (2016), <https://doi.org/10.1007/s12649-015-9455-3>
- ¹¹ S. S. Bagali, B. S. Gowrishankar and A. S. Roy, *Eng. J.*, **3**, 409 (2017), <https://doi.org/10.1016/J.ENG.2017.03.024>
- ¹² A. Blanco, M. C. Monte, C. Campano, A. Balea, N. Merayo *et al.*, in “Handbook of Nanomaterials for Industrial Applications”, Elsevier Inc., 2018, pp. 74-126, <https://doi.org/10.1016/B978-0-12-813351-4.00005-5>
- ¹³ H. Voisin, L. Bergström, P. Liu and A. P. Mathew, *Nanomaterials*, **7**, 57 (2017), <https://doi.org/10.3390/nano7030057>
- ¹⁴ H. J. Kim, J. M. Koo, S. H. Kim, S. Y. Hwang and S. S. Im, *Polym. Degrad. Stab.*, **144**, 128 (2017), <https://doi.org/10.1016/j.polymdegradstab.2017.07.031>
- ¹⁵ S. Mueller, C. Weder and E. J. Foster, *RSC Adv.*, **4**, 907 (2014), <https://doi.org/10.1039/c3ra46390g>
- ¹⁶ R. H. F. Faradilla, G. Lee, A. Rawal, M. H. Stenzel *et al.*, *Cellulose*, **23**, 3023 (2016), <https://doi.org/10.1007/s10570-016-1025-8>
- ¹⁷ A. L. Pereira, D. M. do Nascimento, M. de Sá M. Souza Filho, J. P. S. Morais, N. F. Vasconcelos *et al.*, *Carbohydr. Polym.*, **112**, 165 (2014), <https://doi.org/10.1016/j.carbpol.2014.05.090>
- ¹⁸ D. Lu, Q. Cao, X. Li, X. Cao, F. Luo *et al.*, *Hydrometallurgy*, **95**, 145 (2009), <https://doi.org/10.1016/j.hydromet.2008.05.008>
- ¹⁹ T. Vaughan, C. W. Seo and W. E. Marshall, *Bioresour. Technol.*, **78**, 133 (2001), [https://doi.org/10.1016/S0960-8524\(01\)00007-4](https://doi.org/10.1016/S0960-8524(01)00007-4)
- ²⁰ V. Janaki, B.-T. Oh, K. Shanthi, K.-J. Lee, A. K. Ramasamy *et al.*, *Synth. Met.*, **162**, 974 (2012), <https://doi.org/10.1016/j.synthmet.2012.04.015>
- ²¹ L. S. Silva, F. J. L. Ferreira, M. S. Silva, A. M. G. L. Citó, A. B. Meneguín *et al.*, *Int. J. Biol. Macromol.*, **116**, 1282 (2018), <https://doi.org/10.1016/j.ijbiomac.2018.05.034>
- ²² R. N. Hobson, D. G. Hepworth and D. M. Bruce, *J. Agric. Eng. Res.*, **78**, 153 (2001), <https://doi.org/10.1006/jaer.2000.0631>
- ²³ H. Kalita, A. Hazarika, R. Kandimalla, S. Kalita and R. Devi, *RSC Adv.*, **8**, 36791 (2018), <https://doi.org/10.1039/C8RA04470H>
- ²⁴ S. Elanthikkal, U. Gopalakrishnapanicker, S. Varghese and J. T. Guthrie, *Carbohydr. Polym.*, **80**, 852 (2010), <https://doi.org/10.1016/j.carbpol.2009.12.043>
- ²⁵ W. Chen, H. Yu, Y. Liu, P. Chen, M. Zhang *et al.*, *Carbohydr. Polym.*, **83**, 1804 (2011), <https://doi.org/10.1016/j.carbpol.2010.10.040>
- ²⁶ P. Phanthong, P. Reubroycharoen, X. Hao, G. Xu, A. Abudula *et al.*, *Carbon. Resour. Convers.*, **1**, 32 (2018), <https://doi.org/10.1016/j.crcon.2018.05.004>
- ²⁷ M. V. G. Zimmerman, *J. Reinf. Plast. Compos.*, **35**, 628 (2016), <https://doi.org/10.1177/0731684415626286>
- ²⁸ H. Abrial, V. Lawrensus, D. Handayami and E. Sugiarti, *Carbohydr. Polym.*, **191**, 161 (2018), <https://doi.org/10.1016/j.carbpol.2018.03.026>
- ²⁹ A. Quellmalz and A. Mihranyan, *ACS Biomater. Sci. Eng.*, **191**, 161 (2018), <https://doi.org/10.1021/ab500161x>
- ³⁰ C. Demitri, R. Del Sole, F. Scalera, A. Sannino, G. Vasapollo *et al.*, *J. Appl. Polym. Sci.*, **110**, 2453 (2008), <https://doi.org/10.1002/app.28660>
- ³¹ W. E. Marshall, L. H. Wartelle, D. E. Boler, M. M. Johns and C. A. Toles, *Bioresour. Technol.*, **69**, 263 (1999), [https://doi.org/10.1016/S0960-8524\(98\)00185-0](https://doi.org/10.1016/S0960-8524(98)00185-0)
- ³² C. Kuo, C. Wu and M. Chen, *Desalin. Water Treat.*, **55**, 1264 (2015), <https://doi.org/10.1080/19443994.2014.926460>
- ³³ G. Sinawang, T. Asoh, M. Osaki, H. Yamaguchi, A. Harada *et al.*, *Appl. Polym. Mater.*, **2**, 2274 (2020), <https://doi.org/10.1021/acsapm.0c00250>
- ³⁴ Z. Sheng, Y. Shen, H. Dai, S. Pan, B. Ai *et al.*, *Polym. Compos.*, **37**, 915 (2016), <https://doi.org/10.1002/pc.24140>
- ³⁵ A. L. S. Pereira, D. M. Nascimento, M. de Sá M. Souza Filho, A. Ribeiro Cassales, J. P. S. Morais *et al.*, *Bioresources*, **9**, 7749 (2014), <https://doi.org/10.15376/biores.9.4.7749-7763>
- ³⁶ H. P. S. A. Khalil, Y. Davoudpour, Md. Nazrul Islam, A. Mustapha, K. Sudesh *et al.*, *Carbohydr. Polym.*, **99**, 649 (2014), <https://doi.org/10.1016/j.carbpol.2013.08.069>
- ³⁷ R. Leyva-Ramos, L. E. Landin-Rodriguez, S. Leyva-Ramos and N. A. Medellin-Castillo, *Chem. Eng. J.*, **180**, 113 (2012), <https://doi.org/10.1016/j.cej.2011.11.021>
- ³⁸ N. A. Fakhre and B. M. Ibrahim, *J. Hazard. Mater.*, **343**, 324 (2018), <https://doi.org/10.1016/j.jhazmat.2017.08.043>
- ³⁹ B. Zhu, T. Fan and D. Zhang, *J. Hazard. Mater.*, **153**, 300 (2008), <https://doi.org/10.1016/j.jhazmat.2007.08.050>
- ⁴⁰ S. Pitsari, E. Tsoufakis and M. Loizidou, *Chem. Eng. J.*, **223**, 18 (2013), <https://doi.org/10.1016/j.cej.2013.02.105>
- ⁴¹ G. M. Al-Senani and L. F. Al-Fawzan, *Egypt. J. Aquat. Res.*, **44**, 187 (2018), <https://doi.org/10.1016/j.ejar.2018.07.006>
- ⁴² A. de Sá, A. S. Abreu, I. Moura and A. V. Machado, in “Water Purification. Nanotechnology in the Agri-Food Industry”, edited by A. M. Grumezescu,

Academic Press, 2017, pp. 289-322,
<https://doi.org/10.1016/B978-0-12-804300-4.00008-3>

⁴³ J. Anwar, U. Shafique, W. Zaman, M. Salman, A. Dar *et al.*, *Bioresour. Technol.*, **101**, 1725 (2010),
<https://doi.org/10.1016/j.biortech.2009.10.021>

⁴⁴ M. Arshadi, M. J. Amiri and S. Mousavi, *Water Resour. Ind.*, **6**, 1 (2018),
<https://doi.org/10.1016/j.wri.2014.06.001>

⁴⁵ L. Lü, L. Chen, W. Shao and F. Luo, *Sep. Sci. Technol.*, **47**, 1552 (2012),
<https://doi.org/10.1080/01496395.2011.645984>

⁴⁶ L. Di Palma and R. Mecozi, *J. Hazard. Mater.*, **147**, 768 (2007),
<https://doi.org/10.1016/j.jhazmat.2007.01.072>

⁴⁷ S. B. Chen, Y. B. Ma, L. Chen and K. X. Ian, *Geochem. J.*, **44**, 233 (2010),
<https://doi.org/10.2343/geochemj.1.0065>

⁴⁸ K. S. Low, C. K. Lee and S. M. Mak, *Wood Sci. Technol.*, **38**, 629 (2004),
<https://doi.org/10.1007/s00226-003-0201-9>

⁴⁹ J. Yang, Y. T. Park, K. Baek and J. Choi, *Sep. Sci. Technol.*, **45**, 12 (2010),
<https://doi.org/10.1080/01496395.2010.493782>